B. (1984) *Liebigs Ann. Chem. 5*, 951.
Paulsen, H., Peters, T., Sinnwell, V., Heume, M., & Meyer, B. (1986) *Carbohydr. Res. 156*, 87.
Van Gunsteren, W. F., & Berendsen, H. J. C. (1977) *Mol. Phys. 34*, 1311.
Van Gunsteren, W. F., & Karplus, M. (1982) *Macromolecules 15*, 1528.
Van Gunsteren, W. F., Kaptein, R., & Zuiderweg, E. R. P. (1983) *NATO/CECAM Workshop of Nucleic Acid Conformation/Dynamics*, Orsay, p 79.
Vliegenthart, J. F. G., Dorland, L., & van Halbeek, H. (1983) *Adv. Carbohydr. Chem. Biochem. 41*, 209.
Wüthrich, K., Wider, G., Wagner, G., & Braun, W. (1982) *J. Mol. Biol. 155*, 311.

Solution Conformation of the Branch Points of N-Linked Glycans: Synthetic Model Compounds for Tri′-Antennary and Tetraantennary Glycans†

D. A. Cumming,‡ R. N. Shah,‡ J. J. Krepinsky,§ A. A. Grey,∥ and J. P. Carver*,‡
Departments of Medical Genetics and Medical Biophysics, University of Toronto, Ludwig Institute for Cancer Research, and Toronto Biomedical NMR Centre, Toronto, Ontario, Canada M5S 1A8

Received May 28, 1986; Revised Manuscript Received May 20, 1987

ABSTRACT: The solution conformation of model compounds for the tri′-antennary and tetraantennary (six-arm) branch point of N-linked glycans has been determined through the use of chemical shift, relaxation, and nuclear Overhauser enhancement data. The object was to establish the conformation about the glycosidic linkages in the N-linked substructure GlcNAc(β1,6)[GlcNAc(β1,2)]Man(α)- by estimation of values for the appropriate glycosidic torsional angles. The GlcNAc(β1,6) linkage in a trisaccharide model compound was found to be constrained to a narrow rotameric subpopulation about the substituted Man C5–C6 bond ($\omega = -60°$) and a narrow range of possible $\phi - \psi$ values. Free rotation about the Man C5–C6 bond was obstructed by unfavorable steric interactions between the GlcNAc(β1,6) and GlcNAc(β1,2) residues. A ϕ, ψ value of 55°, 190° was found to be consistent with the NMR data for the GlcNAc(β1,6) linkage. However, the value of ψ appears to be "virtual" in that the molecule is in equilibrium between two different values (90° and 252°). For the GlcNAc(β1,2) linkage, *complete* agreement between all the observed NMR parameters and all the calculated ensemble average values could only be obtained with a set of potential energy functions which included hydrogen bonding. Other choices of potentials yielded calculated values that disagreed with at least two of the observed quantities. As a result, we infer that an interresidue hydrogen bond is formed, and we find it to be between the GlcNAc(β1,2) ring oxygen and the Man C3 hydroxyl. In this conformation the values of ϕ and ψ are restricted to values in the vicinity of 40° and −5°, respectively. This conformation differs from that reported for the same linkage in glycopeptides.

Specification of the solution conformation of glycans has provided valuable insights into their synthesis and biological roles (Lemieux, 1978; Lemieux et al., 1980; Thorgersen et al., 1982; Bock et al., 1982; Carver & Brisson, 1983; Brisson & Carver, 1983a; Rademacher et al., 1983; Montreuil, 1984; Paulsen et al., 1985). Nuclear magnetic resonance spectroscopy (NMR)[1] is especially suited for the determination of the solution conformation of glycans. The NMR parameters of greatest utility to conformational analyses are chemical shifts, coupling constants, relaxation rates, and particularly ^{1}H{^{1}H} NOE's (Lemieux, 1978; Brisson & Carver, 1983b–d; Carver et al., 1987). Unfortunately, direct analysis of the spectra of N-linked glycans is often complicated by spectral overlap and tightly coupled spin systems. To overcome these difficulties, we have previously found it useful to perform conformational analyses on lower molecular weight oligosaccharides, which model substructural elements of larger N-linked glycans (Brisson & Carver, 1983b). This approach has proven particularly useful when specific chemical modification (e.g., deuteriation) of the model compound allows more detailed analysis of complicated spin systems (Cumming et al., 1986). The use of model compounds allows, in NOE experiments, the establishment of a set of expected enhancements. Moreover, an evaluation of the relative contribution of direct and indirect (three-spin) enhancements to the observed NOE signal intensities is facilitated since the NMR spectra of these compounds are intrinsically simpler than those of N-linked glycans.

Thus, prior to embarking on a detailed study of triantennary, tri′-antennary and tetraantennary glycans [for a complete discussion of the various structural classes of N-linked oligosaccharides, see the review of Vliegenthart et al. (1983)], we sought to evaluate the solution conformation of appropriate model compounds. In a forthcoming paper, we will present the results of our study of the conformations about the GlcNAc(β1,2)[GlcNAc(β1,4)]Man(α)- branch point. In this paper, we will present our results on one class of these synthetic compounds, those which model the GlcNAc(β1,2)[GlcNAc-

† This research was supported by Grants MT-3732 and MA-6499 from the Medical Research Council of Canada.
* Address correspondence to this author.
‡ University of Toronto.
§ Ludwig Institute for Cancer Research.
∥ Toronto Biomedical NMR Centre.

[1] Abbreviations: NMR, nuclear magnetic resonance spectroscopy; NOE, nuclear Overhauser enhancement; GlcNAc, 2-acetamido-2-deoxy-D-glucopyranose; Man, D-mannopyranose; FID, free induction decay; SDDS, spin-decoupling difference spectroscopy; T_1, bulk longitudinal relaxation time; Y{X}, NOE observed on nucleus Y upon irradiation of nucleus X.

0006-2960/87/0426-6655$01.50/0

(β1,6)]Man(α1,6) branch point in tri'-antennary and tetraantennary N-linked glycans. In a previous paper (Bock et al., 1982) on an analogous model oligosaccharide, the glycosidic torsional angles were estimated solely by potential energy calculations, the observed NOE's being deemed too small at 400 MHz for interpretation. Moreover, the disubstituted mannose moiety was present as a reducing sugar, thus complicating the interpretation of any potential interresidue NOE's.

Experimental Procedures

Sample Source. Details of the chemical synthesis of all model compounds will be presented elsewhere (Shah et al., unpublished data).

^1H NMR Spectroscopy. Samples were prepared for ^1H NMR spectroscopy by passage over a Chelex (200–400 mesh, Na^+ form, Bio-Rad) column (0.6 × 5 cm) and repeated dissolution/lyophilization from D_2O (99.96 atom %, low in paramagnetic impurities, Aldrich). Finally, the sample was suspended in 0.4 mL of D_2O in an argon atmosphere to a final concentration of approximately 20–30 mM. All NMR experiments were performed on a Nicolet NT-360 spectrometer located at the Toronto Biomedical NMR Centre. Typically, a 90° (8 μs) observe pulse and quadrature phase cycling were used to accumulate 16K data sets over a sweep width of ±1100 Hz. All NMR experiments were performed at an ambient probe temperature of 23 ± 1 °C.

Difference Spectroscopy. NOE and SDDS experiments were performed by difference spectroscopy (Sanders & Mersh, 1983). Data were accumulated as difference FID's prior to Fourier transformation. Steady-state NOE experiments were performed with irradiation times and pulse intervals that were at least 5 times the longest T_1 in the sample. Exponential line broadening factors of 0.1 (for SDDS) to 1.0 Hz (for NOE experiments) were applied to FID's prior to transformation.

T_1 Experiments. Spin–lattice relaxation times were measured by a modification of the inversion–recovery method (Vold et al., 1968), employing a composite 180° pulse for inversion to compensate for pulse imperfections. Twelve values of τ were used and T_1 values determined by a three-parameter fit to the variation in integrated peak intensity (Levy & Peat, 1975).

2-D NMR. Two-dimensional shift-correlated (COSY) spectra were accumulated as 512 FID's, each of 2K data points (real + complex), modulated in t_1 in the usual fashion (Bax, 1982). Data were transferred either via an RS-232 interface (at 1200 baud) to a Vax 11/780 (Ontario Cancer Institute) or via a serial coax line (at 3.5 megabaud) to a DMA interface board attached to a Vax 11/780 (Division of Medical Computing, University of Toronto). After apodization (with a Hanning function), zero filling (as appropriate), and Fourier transformation in both dimensions, a power spectrum was obtained and the data set symmetrized. The final data sets were matrices of 1K × 1K real points with a digital resolution of 1.3 Hz per point in each dimension. All programs for data transfer and processing were written in FORTRAN by Tom Lew (Department of Medical Genetics, University of Toronto).

Spectral Simulations. Simulations of ^1H NMR spectra were performed with utilization of a modified version (Cooper, 1979) of the program LAOCON III (Castellano & Bothner-By, 1963). The program has been further modified by us to facilitate addition of distinct spin sets over a defined spectral region and their display on graphics hardware.

Definition of Glycosidic Torsion Angles. Torsion angles and their angular origins are defined as previously for 1,6 linkages (Tvaroska et al., 1978): ϕ = H1–C1–O1–C6', ψ = C1–O1–C6'–C5', and ω = O1–C6'–C5'–H5', where the primed labels refer to the aglyconic atoms. In other than 1,6 linkages, ψ is defined as C1–O1–CX'–HX'.

Computational Procedure. NOE and T_1 values as a function of glycosidic torsional angles were calculated as described previously (Brisson & Carver, 1983b; Carver et al., 1986). Steric interactions were calculated on the basis of the minimum contact distances between nonbonded atoms (Ramachandran & Sasisekharen, 1968). Atomic coordinates were obtained from either neutron diffraction data for Man(α)OMe (Jeffery et al., 1977) or from X-ray data for GlcNAc(β)-residues (Mo, 1979). Source code listings for NOE, T_1, and potential energy algorithms utilized in these papers are available from the authors.

Results

The structures of the model compounds employed in this study, GlcNAc(β1,6)Man(α)OMe (I) and GlcNAc(β1,6)-[GlcNAc(β1,2)]ManOMe (II), are schematically represented as

I II

Partial 360-MHz ^1H NMR spectra of these compounds are shown in Figure 1A and 3A. Assignment of the Man-H1, GlcNAc-H1, and Man-H2 signals is based on characteristic chemical shifts and coupling constants (Vliegenthart et al., 1983). Of particular interest is the doublet appearing at 4.18–4.2 ppm. The spectral region from 4.0 to 4.3 ppm typically contains only Man-H2 signals; however, on the basis of its apparent coupling constants (including a large coupling of 11.5 Hz), this signal was tentatively assigned as Man-H6. The same assignment was made in an analogous oligosaccharide by Bock et al. (1982). An explanation for its unusual downfield shift position will be presented below.

Quantitative interpretation of $^1H\{^1H\}$ NOE's requires as complete an assignment of the ^1H NMR spectrum as possible. For compounds I and II, SDDS and COSY experiments were employed to assign the chemical shifts (δ) and coupling constants (J) of the remaining protons in each spectrum, confirming the assignment of the 4.2 ppm resonance as Man-H6. Complete assignment of all nonexchangeable protons (30 protons) was possible for compound II by COSY experiments (data not shown). This is a somewhat unusual situation for oligosaccharides and reflects the paucity of tightly coupled spin systems and complicating spectral overlap. The chemical shift and coupling constant data derived from SDDS and COSY experiments are listed in Table I. Spectral simulation of compounds I and II (Table I) resulted in calculated spectra (data not shown) that are in complete agreement with the experimental spectra. More importantly, the magnitudes of the scalar coupling constants listed in Table I are consistent with a $^4C_1$ chair conformation for the constituent monosaccharide rings and give no indication of ring deformation. This is an important consideration for our conformational analysis since it is assumed that the pyranose rings are rigid in solution and possess the geometry found in X-ray or neutron diffraction studies.

Estimation of Rotational Correlation Time. The utility of NMR relaxation processes to estimate internuclear distances derives from the ability to extract the contribution of one mechanism, the dipole–dipole (D–D) mechanism, from the total relaxation of a nuclear magnetic moment. D–D relaxation exhibits an inverse sixth-power dependence on the dis-

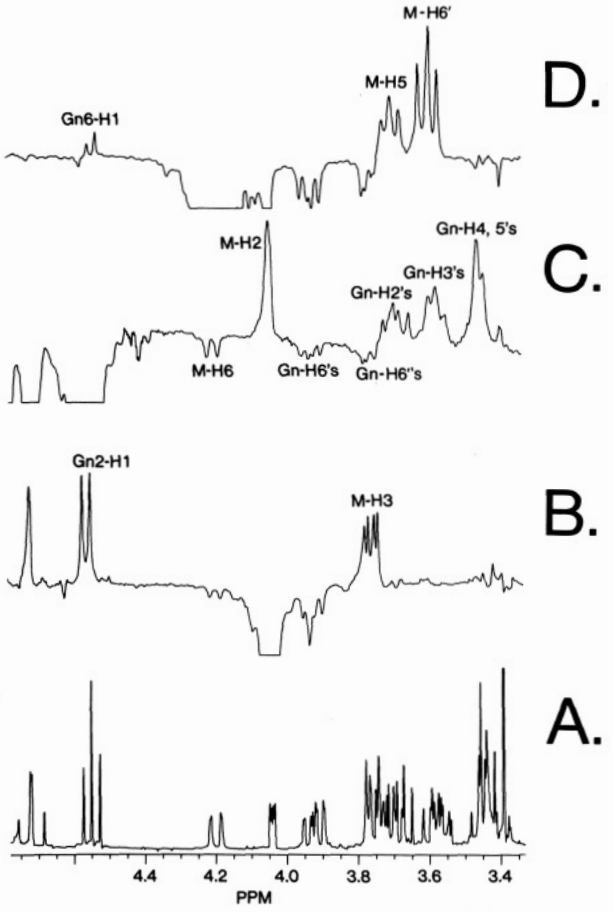

FIGURE 1: Partial 360-MHz NOE difference spectra for compound II. (A) Control spectrum. (B) NOE difference spectrum obtained by irradiation of Man-H2. (C) NOE difference spectrum obtained by irradiation of both GlcNAc-H1's. (D) NOE difference spectrum obtained by irradiation of Man-H6.

tance between, in the case of ^{1}H NMR, an irradiated and any spatially proximal hydrogen. The relative contribution to D–D relaxation for any pair of hydrogens can be measured by nuclear Overhauser enhancements. However, in addition to its distance dependence, D–D relaxation is also modulated by the (random) motional characteristics of the molecule in solution. This molecular motion is characterized by the parameter τ_c, the isotropic rotational correlation time. The sign and maximum theoretical value for any direct NOE is a function of the product of the Larmor frequency (ω_0) and τ_c. At values of $\omega_0\tau_c < 1$, direct NOE's are positive while when $\omega_0\tau_c > 1$ direct NOE's are negative. Indirect NOE's (three-spin effects) are enhancements observed on other spatially proximal nuclei resulting from D–D interactions with a hydrogen experiencing a direct NOE. Three-spin effects are always negative in sign (Noggle & Shirmer, 1971) and may be observed for nuclei remote from the irradiated nucleus.

The rotational correlation time for the samples of compounds I and II was estimated by comparison of observed, conformationally independent intramolecular NOE's and T_1's with values calculated for these parameters as a function of τ_c. For compounds I and II, the GlcNAc-H3{GlcNAc-H1} and GlcNAc-H4,5{GlcNAc-H1} NOE's were employed as well as the GlcNAc-H6 T_1 values. In addition, for compound I, the Man-H2{Man-H1} NOE and the Man-H1 T_1 values were also employed. These data lead to an estimate of τ_c of 2.4×10^{-10} and 3.5×10^{-10} s for compounds I and II, respectively. The rate of internal motion about the glycosidic linkages was assumed to be slow in relation to the overall isotropic tumbling rate as found previously for mono-, di-, and trisaccharides

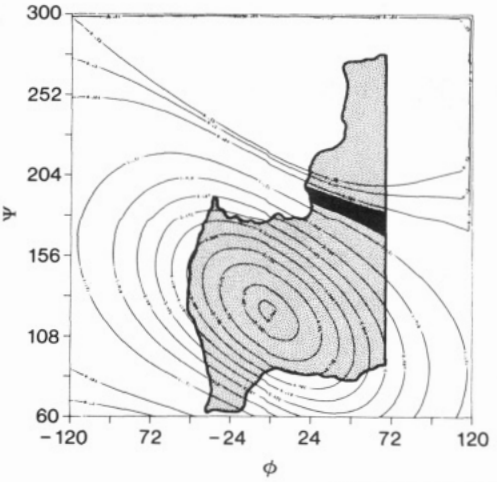

FIGURE 2: A calculated NOE contour surface for the GlcNAc(β1,6) linkage in compound II. NOE (and T_1 values), as a function of ϕ and ψ, were calculated as described previously (Brisson & Carver, 1983b). A 120 × 120 matrix was generated spanning a range of 240° in both ϕ and ψ. The grey-shaded area indicates the sterically allowed values of ϕ and ψ. The solid black region indicates the area where calculated values are within a specified range of the experimentally observed value. For NOE's, the range is defined as the average of the observed ± 2σ (see Table II). For T_1 surfaces, the range is defined as the observed value ± 20%. The 12 contour levels in this (and other) figure(s) are defined as the following percentage of the maximum value in the ϕ–ψ array: 99.0, 95.0, 85.0, 75.0, 65.0, 55.0, 45.0, 35.0, 25.0, 15.0, 5.0, and 3.0%. The contour surface shown here is for the calculated values of the GlcNAc(β1,6)-H1{Man-H6} NOE. The maximum NOE value is 8.8% and occurs near ϕ, ψ = 0°, 120°.

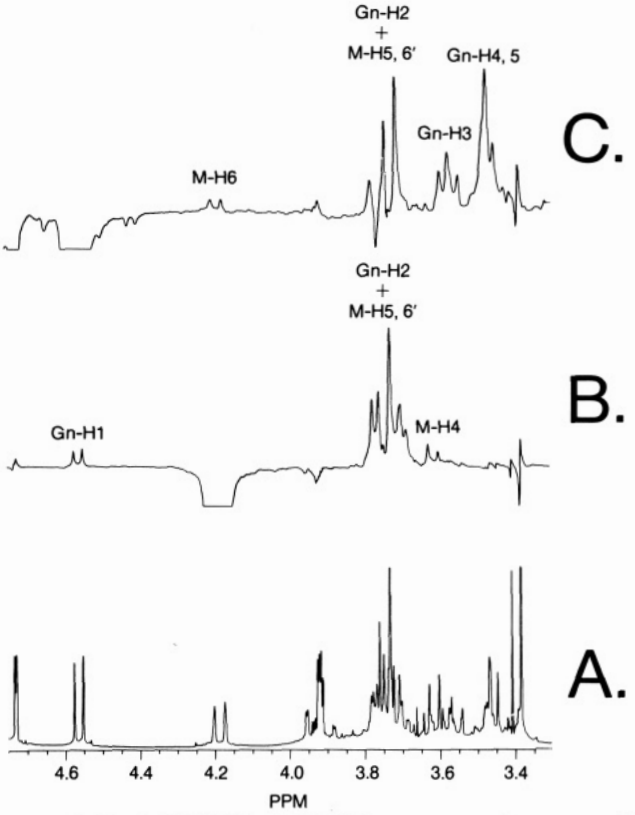

FIGURE 3: Partial 360-MHz NOE difference spectra for compound I. (A) Control spectrum. (B) NOE difference spectrum obtained by irradiation of Man-H6. (C) NOE difference spectrum obtained by irradiation of GlcNAc-H1.

(Brisson & Carver, 1983a,b; Hayes et al., 1982; Cumming & Carver, 1987a). For these values of τ_c at 360 MHz, $\omega_0\tau_c < 1$; direct NOE's are thus positive in sign. At these values of $\omega_0\tau_c$ (~0.7), ^{13}C T_1's are largely insensitive to variations in

Table I: Chemical Shift Assignments for Compounds I and II[a,b]

	Man(α)OMe	GlcNAc6	GlcNAc2
Compound I			
observed			
H1 ($J_{1,2}$)	4.725 (1.4)	4.561 (8.6)	
H2 ($J_{2,3}$)	3.914 (3.6)	3.731 (9.9)	
H3 ($J_{3,4}$)	3.736 (9.3)	3.565 (10.4)	
H4 ($J_{4,5}$)	3.596 (9.3)	~3.44 (c)	
H5 ($J_{5,6'}$)	3.698 (6.4)	~3.47 (5.8)	
H6 ($J_{5,6}$)	4.182 (1.0)	3.935 (1.7)	
H6′ ($J_{6,6'}$)	3.754 (−10.1)	3.759 (−12.6)	
calculated			
H1 ($J_{1,2}$)	4.725 (1.6)	4.562 (9.0)	
H2 ($J_{2,3}$)	3.913 (3.4)	3.734 (10.0)	
H3 ($J_{3,4}$)	3.735 (9.8)	3.567 (10.0)	
H4 ($J_{4,5}$)	3.600 (10.0)	3.452 (8.5)	
H5 ($J_{5,6'}$)	3.702 (6.7)	3.475 (5.9)	
H6 ($J_{5,6}$)	4.180 (1.4)	3.935 (1.5)	
H6′ ($J_{6,6'}$)	3.748 (−10.5)	3.760 (−12.5)	
Compound II			
observed			
H1 ($J_{1,2}$)	4.717 (1.3)	4.534 (8.4)	4.558 (8.3)
H2 ($J_{2,3}$)	4.036 (3.4)	3.711 (10.2)	3.668 (10.3)
H3 ($J_{3,4}$)	3.755 (9.6)	3.566 (8.9)[b]	3.572 (8.9)[b]
H4 ($J_{4,5}$)	3.415 (9.7)	~3.44 (c)	~3.43 (c)
H5 ($J_{5,6'}$)	3.693 (9.0)	3.429 (4.5)	3.455 (4.5)
H6 ($J_{5,6}$)	4.193 (1.2)	3.907 (1.5)	3.930 (1.0)
H6′ ($J_{6,6'}$)	3.587 (−10.8)	3.748 (−12.4)	3.748 (−12.3)
calculated			
H1 ($J_{1,2}$)	4.717 (1.4)	4.535 (8.8)	4.558 (8.6)
H2 ($J_{2,3}$)	4.038 (3.3)	3.714 (10.8)	3.670 (10.2)
H3 ($J_{3,4}$)	3.756 (9.4)	3.568 (8.6)	3.570 (8.2)
H4 ($J_{4,5}$)	3.417 (9.2)	3.453 (8.9)	3.439 (9.3)
H5 ($J_{5,6'}$)	3.691 (8.8)	3.427 (5.6)	3.460 (5.5)
H6 ($J_{5,6}$)	4.196 (1.8)	3.909 (1.4)	3.931 (1.0)
H6′ ($J_{6,6'}$)	3.590 (−10.9)	3.754 (−12.1)	3.754 (−12.0)
Other Signals			
N*Ac* (compound I)		2.037	
N*Ac* (compound II)		2.019	2.059
O*Me* (compound I)	3.381		
O*Me* (compound II)	3.387		

[a] Chemical shifts are given in ppm referenced indirectly to DSS, through acetone at 2.225 ppm. Average error for chemical shifts is considered to be 0.003 ppm; digital resolution of spectra is 0.25 Hz per point. Coupling constants appear in parentheses and are given in hertz. [b] Chemical shift values for tightly coupled spin systems were estimated from COSY cross-peak positions. [c] First-order approximation of coupling constant could not be obtained due to tight coupling.

τ_c and were therefore not employed.

Determination of the Torsional Angles for the GlcNAc-(β1,6) Linkage. Three torsional angles (ϕ, ψ, and ω) are sufficient to describe the solution conformation of the GlcNAc(β1,6) linkage. As previously described for 1,6 linkages (Brisson & Carver, 1983a,b), a value for the torsional angle ω for this linkage can, in principle, be estimated from analysis of the multiplet patterns of the Man-H5 and -H6′ protons as well as from the magnitude of observed interresidue $^1H\{^1H\}$ NOE's. For 1,6 linkages, three conformations corresponding to ω = 180°, −60°, and +60° (gauche–gauche, gauche–trans, and trans–gauche respectively) define rotameric subpopulations about the C5–C6 bond. For linkages to mannopyranoses, one of these rotamers (ω = +60°) is unfavorable due to a syn-axial interaction (Hassel–Ottar effect) between O4 and O6 (Marchessault & Perez, 1979; Hassel & Ottar, 1947) and therefore is usually not considered. Estimation of the relative populations of the rotamers defined by ω = −60° and 180° can be obtained from the observed multiplet pattern of Man-H5 and Man-H6′ (Brisson & Carver, 1983a). Visualization of the Man-H5,H6′ multiplet pattern in compound II can be accomplished by irradiation of the Man-H6 hydrogen (Figure 1D), resulting in strong intraresidue enhancements of the Man-H5 and Man-H6′ signals. Comparison of the observed multiplicities with expected patterns, together with the observed $J_{5,6'}$ of ~9 Hz, indicates that a single rotameric subpopulation corresponding to ω = −60° is present in this compound. A similar conclusion was drawn from the COSY spectrum where the cross-peaks assigned to Man-H5/Man-H6 and Man-H6′/Man-H6 exhibit apparent triplet multiplicities (data not shown).

The finding of a single value of ω = −60° in the β1,6 linkage of compound II is somewhat surprising since potential energy calculations indicate that each rotamer is sterically allowable and generates a favorable potential energy surface [see Cumming and Carver (1987b)], although the ω = 180° rotamer is more sterically and energetically constrained. Thus, in the absence of stabilizing or steric interactions, both rotamers should be present in approximately equal amounts, a situation previously observed in another trisaccharide possessing a 1,6 linkage (Brisson & Carver, 1983b). This was more nearly the case for compound I. Analysis of the Man-H5, -H6, and -H6′ multiplicities for compound I was possible only by spectral simulation since the H5 and H6′ signals are tightly coupled (see Table I). A $J_{5,6'}$ value of 6.4 Hz was calculated, which is consistent with the presence of a mixture of C5–C6 rotamers in solution. This indicates that formation of the GlcNAc(β1,2) linkage (leading to compound II) interferes with free interconversion between the two C5–C6 rotamers. This was confirmed by molecular modeling, which shows that, for compound II [GlcNAc(β1,6), ϕ and ψ = 55° and 190°; GlcNAc(β1,2), ϕ and ψ = 40° and −5° (see below)], rotation from ω = −60° to ω = 180° results in severe contact between the GlcNAc2 and GlcNAc6 *N*-acetyl groups near ω = −90°. Rotation through 240° in the opposite direction results in, near ω = +60°, unfavorable steric interactions between either the GlcNAc(β1,2)-H2 and the GlcNAc(β1,6) methyl carbon (when ψ is near 250°) or the GlcNAc(β1,6)-C5 and Man-O4 (when ψ is near 90°). In contrast, for compound I the potential energy profile obtained by holding ϕ and ψ constant (at ϕ and ψ = 50° and 170°) and varying ω shows a rotational barrier of only about 1.5 kcal/mol between ω = 180° and −60° reaching a maximum at ω = −120° [see Cumming and Carver (1987a,b) for a more detailed analysis of ω interconversion].

The remaining torsional angles, ϕ and ψ, for the GlcNAc-(β1,6) linkage can be estimated through quantitative interpretation of $^1H\{^1H\}$ NOE's and conformationally sensitive T_1's. For compound II, the set of conformationally sensitive data was found to consist of the Man-H6′{Man-H6} and GlcNAc6-H1{Man-H6} NOE's and the T_1 of the GlcNAc6-H1. The NOE data were obtained from the experiment shown in Figure 1D. Because $\omega_0\tau_c < 1$, positive NOE signals are observed when direct NOE's dominate whereas negative signals arise when three-spin (indirect) effects predominate. Thus, the net enhancement observed on any hydrogen can be the sum of positive and negative contributions.

As can be seen in Figure 1D, steady-state irradiation of the Man-H6 signal yields positive enhancements on Man-H5, Man-H6′, and GlcNAc6-H1. The low-field component of the Man-H5 multiplet is slightly distorted due to partial overlap of the Man-H3 multiplet, which exhibits three-spin effects due to the direct NOE to the Man-H5 hydrogen. A portion of the negative Man-H3 signal is observed immediately downfield of the Man-H5 signal. Calculations indicate that a small, positive enhancement to the GlcNAc6-H2 is buried beneath

Table II: Summary of NOE and T_1 Data[a]

saturated signal	detected signal	N2	T_1 (obsd) (s)	range (±20%) (s)	T_1 (calcd)[b] (s)	NOE (%) obsd	NOE (%) calcd	rel NOE obsd	rel NOE calcd	rel NOE SD
				Compound I						
GlcNAc6-H1	GlcNAc-H3	5	1.01	0.20	1.03	5.7	6.5	1.0	1.0	0.59
	Man-H6		0.24	0.05	0.23	1.6	1.4	0.28	0.22	0.24
	GlcNAc-H2 + Man-H5,6′		nd[c]	nd	1.46	7.4	8.5	1.30	1.31	0.79
	GlcNAc-H4,5		nd	nd	0.52	10.3	10.4	1.82	1.60	0.29
Man-H6	Man-H6′ + Man-H5	6	nd	nd	0.68	30.3	29.3	1.0	1.0	0.76
	GlcNAc6-H1		0.43	0.09	0.44	1.8	2.6	0.06	0.09	0.30
				Compound II						
GlcNAc-H1	GlcNAc-H2	5	nd	nd	1.52	2.8	2.7	1.0	1.0	0.48
	GlcNAc-H3		nd	nd	1.06	4.0	3.7	1.43	1.36	0.96
	GlcNAc-H4,5		nd	nd	0.52	5.6	5.5	2.01	2.04	0.97
	Man-H2	4	0.80	0.16	0.51	7.6	6.7	3.12	2.48	1.4
Man-H2	Man-H1	3	0.87	0.17	0.80	4.2	4.3	1.0	1.0	0.98
	Man-H3		nd	nd	0.89	5.3	6.6	1.25	1.51	1.2
	GlcNAc2-H1		0.47	0.09	0.46	5.0	6.0	1.19	1.38	0.63
Man-H6	Man-H6′	3	nd	nd	0.22	9.4	10.8	1.0	1.0	0.66
	Man-H5		nd	nd	0.69	7.5	5.0	0.80	0.45	1.4
	GlcNAc6-H1		0.47	0.09	0.48	0.6	0.5	0.06	0.05	0.07
Man-H1	Man-H2	3	0.80	0.16	0.51	3.3	2.8	1.0	1.0	0.60
	O-CH3		0.73	0.15	0.53	4.2	3.9	1.28	1.39	0.46

[a] NOE values expressed as the fractional intensity change relative to the intensity of the saturated signal of one proton (−100.0). Listed NOE values are the average of N2 experiments, and SD is the standard deviation. [b] Calculated values for the NOE's were determined with the glycosidic torsion angles for each linkage determined in this study. [c] nd not determined due to spectral overlap with other signals or tight coupling.

the Man-H5 enhancement but is only on the order of 6% of the Man-H5 intensity and is less than the experimental error in observing the Man-H5{Man-H6} NOE. A small positive enhancement is observed across the glycosidic bond to the GlcNAc6-H1. The intensity of the low-field transition line of the GlcNAc6-H1 signal is reduced since the GlcNAc2-H1 signal exhibits a small negative enhancement and the upfield transition line of the GlcNAc2-H1 overlaps the low-field transition line of the GlcNAc6-H1 signal. It should be noted that the reverse experiment, simultaneous irradiation of GlcNAc6-H1 and GlcNAc2-H1 (Figure 1C), yields a negative enhancement of the Man-H6 proton. In this experiment, the Man-H6 does indeed receive a direct contribution from the irradiated hydrogens, but three-spin contributions via the Man-H6′ and Man-H5 hydrogens together are larger in magnitude (and opposite in sign). Thus, an overall negative enhancement is observed on this hydrogen. This particular enhancement was not used for our conformational analysis since the decoupler power level used to saturate the GlcNAc-H1 signals was higher than that used for other NOE experiments (see below). This results in a small, unmeasurable degree of cross-irradiation on the Man-H6 hydrogen. Since the magnitude of the observed Man-H6 signal is small, the relative contributions from Overhauser enhancement and cross-irradiation could not be quantified. Values for the observed enhancements are listed in Table II.

Computed NOE's and T_1's corresponding to the elements of the conformationally sensitive data set were calculated (see Experimental Procedures) as a function of ϕ and ψ with ω set to −60°. Figure 2 shows the contour map generated for the GlcNAc6-H1{Man-H6} NOE. The region of the ϕ–ψ surface in which calculated values for this NOE fall within the observed experimental limits (as defined in the figure legend) is shaded black. This region defines a bounded subset of the ϕ–ψ surface, which contains an infinite number of possible ϕ–ψ values satisfying that particular experimental result. Similar maps were generated for the other conformationally sensitive relaxation data (i.e., the Man-H6′{Man-H6} NOE and the GlcNAc6-H1 T_1) yielding distinct bounded subsets of the ϕ–ψ surface (data not shown). The region of the ϕ–ψ surface defined by the intersection of these three bounded surfaces constitutes the "experimentally determined solution conformation" of the GlcNAc(β1,6) linkage; i.e., the predicted NOE and T_1 values for any single conformation (with ϕ and ψ falling within this region) are in agreement with all the observed values. In this case, the intersection surface is closely approximated by the blackened region depicted in Figure 2. The range of possible ϕ values is centered about 40° as is typical for GlcNAc(β) linkages. More surprising is that the determined value of ψ is confined to a narrow range centered on 190°. Potential energy calculations predict a wide range of possible ψ values represented by several local energy minima [see Cumming and Carver (1987b)]. To rationalize our experimental results with these calculations, it is necessary to postulate either that important interaction terms are being neglected in the potential energy calculations or that the experimentally determined conformation is a "virtual" conformation (Jardetzky, 1980) representing an average among the conformers defined by the multiple potential energy minima and corresponding to the conformation of, at best, a small fraction of the population of molecules in solution. On the basis of the results presented in the following papers in this series (Cumming & Carver, 1987a,b), we conclude that the latter postulate is applicable here.

Compound I exhibits an even greater degree of conformational mobility than compound II, again resulting in the definition by NMR of a virtual conformation [see Cumming and Carver (1987a)]. The conformationally sensitive data that define the torsion angles of the GlcNAc(β1,6) linkage in compound I consist of the GlcNAc-H1{Man-H6}, (Man-H5 + Man-H6′ + GlcNAc-H2){GlcNAc-H1}, and Man-H6{GlcNAc-H1} NOE's and the GlcNAc-H1 T_1. The necessary NOE data are extracted from the experiments shown in Figure 3. The NOE difference spectrum obtained by irradiation of the Man-H6 signal at 4.182 ppm is shown in Figure 3B. A small interresidue enhancement is observed to the GlcNAc-H1 hydrogen at 4.558 ppm. In addition, positive enhancements are observed to the Man-H5,H6′ tight complex and to Man-H4. While these latter NOE's are in fact conformationally sensitive, the regions of the ϕ–ψ surface defined by these enhancements are so large as to be of only marginal value in defining the conformation of the GlcNAc(β1,6) linkage. Ir-

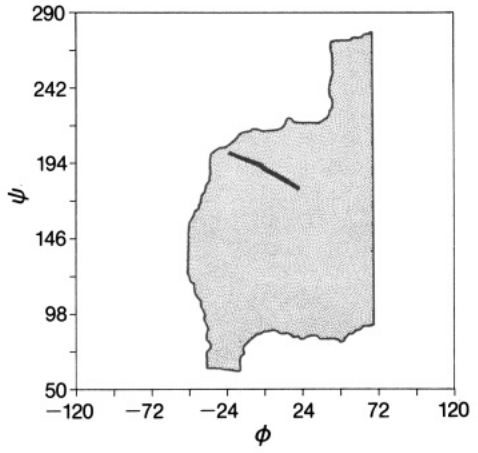

FIGURE 4: Intersection surface for the GlcNAc(β1,6) linkage in compound I. The intersection surface is defined in the text. The illustrated intersection surface was obtained from values of NMR relaxation data calculated as a function of ϕ and ψ with ω fixed at −60°. A similar intersection surface was obtained from data calculated with ω = 180°.

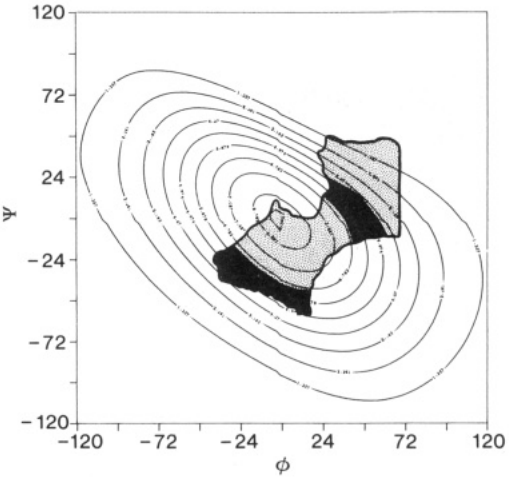

FIGURE 5: A calculated NOE contour surface for the GlcNAc(β1,2) linkage in compound II. Details of the presentation of this surface are described in the legend to Figure 2. The surface for the Man-H2{GlcNAc-H1} NOE is shown. The maximum NOE of 9.8% occurs near ϕ, ψ = 0°, 0°. The intersection surface resulting from consideration of all the conformationally sensitive relaxation data for this linkage is qualitatively similar to the black regions shown in this figure.

radiation of the GlcNAc(β1,6)-H1 yields the NOE difference spectrum shown in Figure 3C. Large, positive intraresidue enhancements are observed to the GlcNAc-H4,5 tight complex and to the GlcNAc-H3. The large enhancement centered at 3.73 ppm is composed of the expected intraresidue NOE to the GlcNAc-H2 and an interresidue NOE to the Man-H5,6′ tight complex. The apparent multiplicity of the constituent signals is further distorted due to an indirect (three-spin) enhancement to the GlcNAc-H6′ mediated by the direct NOE to the GlcNAc-H4,5 tight complex. Since the magnitude of the enhancements to GlcNAc-H2 and GlcNAc-H6′ are a function only of the correlation time and are conformationally independent, the integrated intensity of this entire spectral region (the sum of the GlcNAc-H2, GlcNAc-H6′, and Man-H5,6′ signals) may be mapped as a conformationally sensitive function of the ϕ–ψ surface.

Once again, computed NOE's and T_1's for these parameters were calculated as a function of ϕ and ψ. Contour surfaces were generated for each of the conformationally sensitive parameters with ω fixed at −60°. The resulting "intersection surface" is shown in Figure 4. A similar set of surfaces were generated with ω = 180°, and an almost identical intersection surface was obtained (data not shown). The derived intersection surfaces each encompass a set of possible ϕ–ψ values centered at 0°, 185°. A value for ϕ of 0° is quite unusual for β-linked hexopyranosides; typically, a value closer to +50° would be anticipated (Lemieux, 1978; Brisson & Carver, 1983a–d). As will be discussed below (and treated in more detail in the accompanying papers), the experimentally determined values for ϕ–ψ again result from conformational averaging over the ϕ–ψ–ω surface. Thus, this experimentally determined conformation is also virtual (Jardetzky, 1980).

Determination of the Torsional Angles for the GlcNAc-(β1,2) Linkage. Two glycosidic torsional angles, ϕ and ψ, are sufficient to define the solution conformation about a GlcNAc(β1,2) linkage. For compound II, two sets of interresidue NOE's can be obtained that allow estimates of these angles to be made: those observed upon irradiation of the GlcNAc2-H1 and those obtained upon irradiation of Man-H2. Panels B and C of Figure 1 show the NOE difference spectra obtained in these two experiments. In Figure 1B, irradiation of the Man-H2 signal yields positive enhancements to Man-H1, Man-H3, and GlcNAc2-H1. For the experiment shown in Figure 1C, both GlcNAc H1 signals were fully saturated to avoid problems arising from partial saturation and cross-irradiation, which occurred when irradiation of a single H1 was attempted. In the case of compound II, co-irradiation of the GlcNAc-H1 signals did not preclude measurement of the Man-H2{GlcNAc2-H1} NOE on the basis of the following: (1) NOE experiments on compound I show that irradiation of the GlcNAc6-H1 yields only a negligible enhancement to the Man-H2 signal (Figure 1C). (2) Analysis of the nuclear magnetic relaxation matrix calculated for compounds I and II upon irradiation of the GlcNAc6-H1 [over the range of sterically allowed GlcNAc(β1,6) torsion angles] shows that the Man-H1, Man-H2, and Man-H3 hydrogens do not experience any significant cross-relaxation. Therefore, the Man-H2{GlcNAc2-H1 + GlcNAc6-H1} NOE can be considered to have arisen solely from irradiation of the GlcNAc2-H1 hydrogen. The other positive signals observed in Figure 1C arise from the anticipated intraresidue NOE's to the GlcNAc-H2,H3 and -H4,H5 tight complex. The negative signals at approximately 3.92 and 3.76 ppm are the H6 and H6′ signals of the two GlcNAc residues and are indirect enhancements resulting from the large direct NOE's to the two GlcNAc-H4,H5 tight complexes. The latter enhancement to the H6′ hydrogens partially overlaps the GlcNAc-H2 enhancement resulting in some distortion of the observed signal. Table II catalogs the observed enhancements from Figure 1B,C.

The set of conformationally sensitive parameters for the GlcNAc(β1,2) linkage thus consists of the Man-H2-{GlcNAc2-H1} and GlcNAc2-H1{Man-H2} NOE's and the T_1 for Man-H1. Values for these conformationally sensitive parameters were then calculated as a function of ϕ and ψ. Figure 5 illustrates the results obtained for the Man-H2-{GlcNAc-H1} NOE. Again, the stippled region defines the region of sterically allowed ϕ–ψ values, and the black region defines the subset of the sterically allowed region for which the calculated NOE or T_1 value is within error limits of the observed value. In combination with the other conformationally sensitive data, an intersection surface can again be defined, which is closely approximated by the black regions in Figure 5. Thus, two regions of intersection are now found that again define two subsets of the ϕ–ψ surface and that constitute the experimentally derived solution for the con-

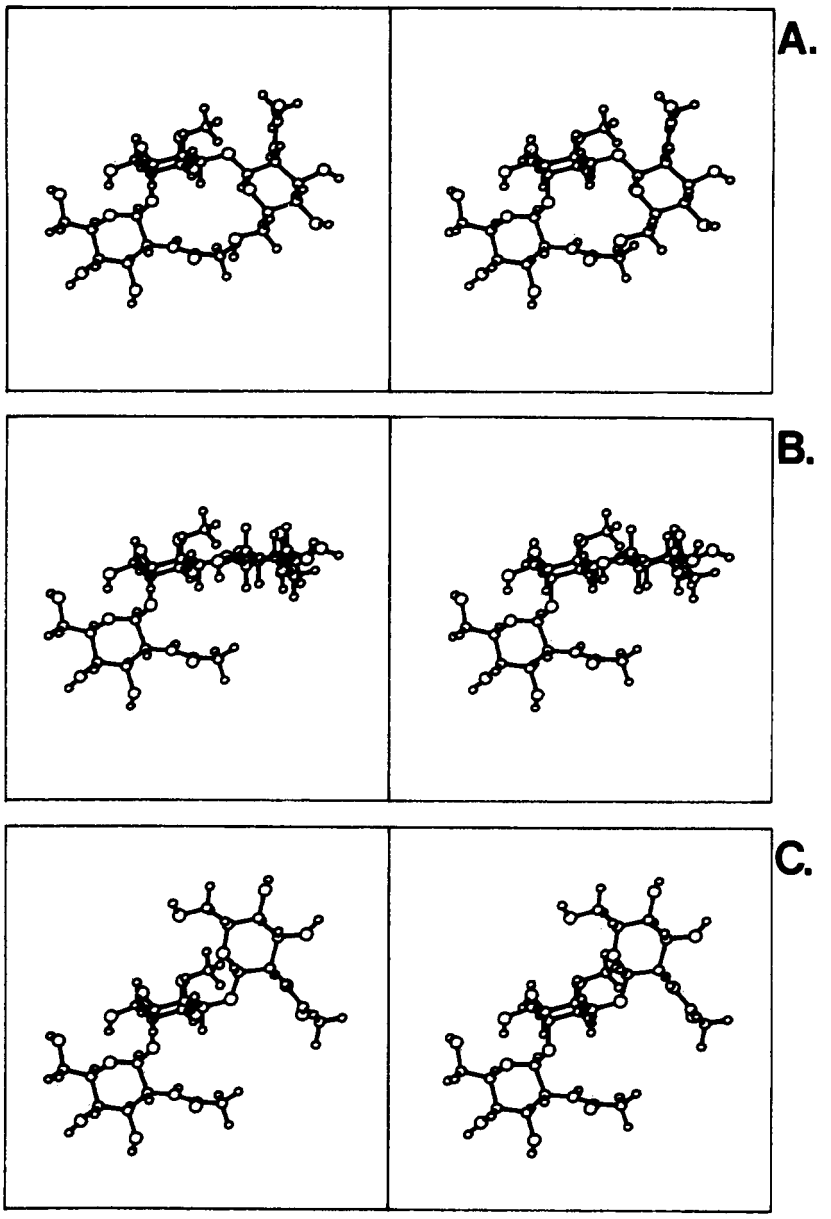

FIGURE 6: Stereo diagrams of the trisaccharide, compound II. Stereo diagram of the trisaccharide model compound, showing the experimentally determined linkage conformations in (B). The relative disposition of the constituent monosaccharides is most clearly seen in panel C where the GlcNAc(β1,2) residue is at the lower left, the disubstituted mannose residue in the center and nearly edge on, and the GlcNAc(β1,6) residue in the upper right. For the GlcNAc(β1,2) linkage, the determined ϕ, ψ values of 40°, −5° are used. Note the hydrogen bond between the Man C3 hydroxyl and the GlcNAc(β1,2)-O5. The linkage conformation of the GlcNAc(β1,6) linkage is specified by the experimentally determined values of ϕ, ψ, ω = 55°, 190°, −60° (panel B); the ϕ = 55° value is within the experimental range of values and is the minimum energy value observed with potential energy calculations [see Cumming and Carver (1987b)]. The experimental GlcNAc(β1,6) linkage conformation is the result of averaging in ψ, in the simplest case between two conformations corresponding to potential energy minima when ψ = 252° (panel A) and ψ = 90° (panel C). Note the proximity of the GlcNAc(β1,6) ring oxygen to Man-H6 in panel A.

formation of the GlcNAc(β1,2) linkage in compound II. For clarity's sake, we will denote the bounded region that encompasses only positive values of ϕ as solution a and the other bounded region as solution b. At torsion angle values within the region specified by solution a, an interresidue hydrogen bond can form between the Man C3 hydroxyl and the ring oxygen of the GlcNAc(β1,2) (O···O distance of 2.78 Å at ϕ, ψ = 40°, −5°). This hydrogen bond contributes significant stabilization energy to this conformer, and its inclusion in potential energy calculations results in a new global minimum overlapping solution a. If hydrogen-bond interactions are omitted from potential energy calculations, the NMR-derived solution conformations do not overlap any energy minima [see Cumming and Carver (1987a)]. Therefore, we tentatively conclude that solution a defines the solution conformation for this linkage [see Cumming and Carver (1987a) for further discussion of this conclusion].

Molecular Models for the Tri' Branch Point in Oligosaccharides and Glycopeptides. Figure 6 summarizes the results of this study by depicting the NMR-determined conformation of compound II. In Figure 6B the values utilized for ϕ and ψ are those determined from NMR and therefore correspond to a virtual conformation. In Figure 6A,C, on the other hand, we have used ϕ, ψ values corresponding to the minimum energy structures between which the 1,6 linkage is averaging [see Cumming and Carver (1987b)]. In Figure 6, hydrogen-bond formation between the GlcNAc(β1,2) ring oxygen and the Man C3 hydroxyl can be seen. In addition, inspection of Figure 6 allows rationalization of the large downfield shift observed in compounds I and II for the Man-H6 signal. In Figure 6A the Man-H6 hydrogen is seen to be proximal to both the GlcNAc(β1,6) ring oxygen (2.60

Å) and to the Man-O4 oxygen (2.62 Å). The downfield displacement for the chemical shift of this hydrogen is thus most likely due to oxygen electron orbital induced deshielding. The Man-O4 seems an unlikely candidate as a source of this deshielding since the hydroxyl group is rotationally averaging and C6 glycosidation in other compounds [e.g., Man(α1,6)-Man(α)-, Man(α1,6)Man(β)-, or in $Man_5GlcNAc_2Asn$ glycopeptides] in fact yields an upfield shift for H6 of 0.12 ppm relative to unsubstituted Man residues (Brisson & Carver, 1983d; Cumming & Carver, 1987b). Hence, it is the proximity of the GlcNAc(β1,6) ring oxygen to the Man-H6, as seen in Figure 6A, that is the most likely source of the observed deshielding.

Discussion

The solution conformation of oligosaccharide models for the six-arm branch point of tri′-antennary and tetraantennary glycans has been investigated. The trisaccharide model GlcNAc(β1,2)[GlcNAc(β1,6)]Man(α)OMe (compound II) was found to possess a considerable degree of secondary structure. Most importantly, the GlcNAc(β1,6) glycosidic torsional angle ω was found to be restricted to a narrow range of values near −60° due to steric interactions with the acetamido moiety of the GlcNAc(β1,2) residue. This result has important biological consequences since, in previous experimental studies of glycans possessing 1,6 linkages, the torsional angle ω is a major determinant in specifying the gross conformation of the glycan (Brisson & Carver, 1983a–d; Carver et al., 1986). Values for the other GlcNAc(β1,6) torsional angles, ϕ and ψ, were found to be confined to a narrow subset of the ϕ–ψ surface. However, since the determined values for the angles either did not correspond to calculated potential energy minima [see Cumming and Carver (1987a,b)] or corresponded to only one of several quasi-equivalent minima (depending on the choice of potential energy algorithm), the occurrence of conformational averaging over the energy surface is indicated. Such averaging of ϕ and ψ is also found to occur for the disaccharide GlcNAc(β1,6)Man(α)OMe [see Cumming and Carver (1987a)]. Thus, values for the GlcNAc-(β1,6) linkage of ϕ, ψ = 40°, 190° in compound II and values of ϕ, ψ = 0°, 190° in compound I specify what have been termed virtual conformations (Jardetzky, 1980; Jardetzky & Roberts, 1982).

The conformation we observe for the GlcNAc(β1,2) linkage in compound II is clearly different than that previously reported for the GlcNAc(β1,2) linkage in hybrid- and complex-type N-linked glycopeptides (Brisson & Carver, 1983c). While the observed values of ϕ are comparable in both cases, the values of ψ differ by 35°. This difference correlates with the formation of an interresidue hydrogen bond at the conformation discerned in this study (ϕ, ψ = 40°, −5°), while ϕ, ψ = 40°, 30° corresponds to the potential energy minimum calculated with the HSEA algorithm. Since the experimental evidence obtained with glycopeptides is inconsistent with the hydrogen-bonding conformation, we conclude that the formation of this hydrogen bond is not energetically favorable in these glycans. One possible reason for this is that the Man(α1,3) C3 hydroxyl or the GlcNAc(β1,2) ring oxygen (or both) might be involved in solvent interactions, for example, by intermolecular hydrogen bonding.

The finding of an interresidue hydrogen bond that stabilizes the GlcNAc(β1,2) linkage in compound II has other important biological consequences. As mentioned above, previous experimental studies have shown that the highest degree of conformational mobility rests with the Man(α1,6) linkage to the core β-linked Man. This flexibility was found to be mainly manifested in various values for ω in this linkage. The core [Man(β1,4)GlcNAc(β1,4)GlcNAc(β)Asn] is believed to be a planar, rigid substructure stabilized by a number of interresidue hydrogen bonds. The Man(α1,3) arm (also glycosidically linked to the β-Man) is another possible site of conformational flexibility but apparently remains invariant in a large number of structures (Brisson & Carver, 1983c). The postulated hydrogen bonding between the antennal Gal(β1,4) to GlcNAc(β1,2) and GlcNAc(β1,2[4]) to Man(α) residues implies a high degree of segmental constraint on the arms on N-linked glycans. An implication of this hypothesis is that the solution conformation of N-linked glycans is largely a property of the torsional angles at a very few glycosidic linkages (Montreuil et al., 1978). This is consistent with the results of this study. The Man(α1,6) linkage can exhibit flexibility about two glycosidic torsion angles (i.e., ω and ψ interconversion). However, the limited degree of flexibility found in compound II argues that extension of the Man(α1,6) arm in tri′-antennary and tetraantennary glycans by a GlcNAc(β1,6) linkage adds only a single source of additional conformational flexibility, averaging in ψ. Our calculations of the most energetically favorable conformers in a tri′ glycopeptide (Cumming and Carver, unpublished observations) suggest that even ψ and ω averaging may not be occurring in the 1,6 linkages of these glycans. Detailed studies of tri′-antennary and tetraantennary glycans are necessary to evaluate this hypothesis. As the next step toward this goal, studies on derivatives of compound II with elongated reducing and nonreducing termini are in progress.

Of considerable interest is the absence in the literature of any report of the appearance of an Man-H6 signal near 4.2 ppm in tetraantennary N-linked glycans (Vliegenthart et al., 1984; van Halbeek et al., 1981; Fournet et al., 1978) or tri′-antennary oligosaccharides (Michalski et al., 1982). The relative intensity of assigned signals in this spectral region of N-linked glycopeptides precludes the possibility that the Man-H6 signal is buried beneath another. This allows for two interesting possibilities. First, further substitution of the GlcNAc(β1,6) arm results in shielding of Man-H6. This is an intriguing possibility since it would provide an additional tool to assess the glycan conformation along this arm. However, Bock et al. (1982) observed that further arm substitution with Gal(β1,4) residues in a trisaccharide analogous to our compound II neither significantly altered the chemical shift of the Man H6 nor altered the value for the Man(α) $J_{5,6'}$. Second, and not necessarily exclusive of the first possibility, altered secondary structure exists in biologically derived N-linked glycans. One variant of this hypothesis is that the GlcNAc(β1,2) conformation on the tri′ branch is altered, allowing free rotation about the GlcNAc(β1,6) linkage. This is unlikely though, since the model compound I employed in this study still exhibits the downfield displacement of Man-H6. A more likely explanation stems from consideration of the source of the Man-H6 downfield shift. The proximity of the Man-H6 to the deshielding effects of the GlcNAc(β1,6) ring oxygen is dependent not only on the value of ω but also on the values of ϕ and ψ. Since conformational averaging has been implicated in the observed value for ψ (190°) in compound II, this raises the possibility that restricting the allowed values of ψ (e.g., near +120°) could result in an increased interatomic distance between Man-H6 and GlcNAc-O5, to the extent that deshielding of Man-H6 no longer occurs (Figure 6C). Direct calculation of the GlcNAc-O5···Man-H6 distance as a function of ψ shows an increase in the interatomic distance as ψ decreases from 190° although the geometric relationship between

GlcNAc-O5 and Man-H6 should also be considered. In addition, potential energy minimization calculations for a tri′ glycopeptide (Cumming and Carver, unpublished observations) support this conclusion. For all calculated conformers, the GlcNAc(β1,6) ψ values were less than 170°, and most were found to be near $\psi = 110°$. We therefore conclude that, in the tri′-antennary and tetraantennary glycans analyzed to date by ^{1}H NMR, the ψ value for the GlcNAc(β1,6) linkage is restricted to values near 110°. This conclusion, if substantiated, imposes an even higher degree of conformational rigidity upon the tri′ branch point of N-linked glycans than demonstrated with the chemically synthesized model fragments.

ACKNOWLEDGMENTS

We thank Dr. Brad Bendiak, Dr. James Rini, Marlene Stubbs, and Stephen Michnick for critical review and comment on this work.

Registry No. I, 80264-88-6; II, 109976-96-7.

REFERENCES

Bax, A. (1982) *Two Dimensional Nuclear Magnetic Resonance in Liquids*, Reidel, Boston.

Bock, K., Arnarp, J., & Lonngren, J. (1982) *Eur. J. Biochem. 129*, 171–178.

Brisson, J. R., & Carver, J. P. (1983a) *Can. J. Biochem. Cell Biol. 61*, 1067–1078.

Brisson, J. R., & Carver, J. P. (1983b) *Biochemistry 22*, 1362–1368.

Brisson, J. R., & Carver, J. P. (1983c) *Biochemistry 22*, 3671–3679.

Brisson, J. R., & Carver, J. P. (1983d) *Biochemistry 22*, 3680–3686.

Carver, J. P., & Brisson, J. R. (1984) in *Biology of Carbohydrates* (Ginsburg, V., & Robbins, P. W., Eds.) pp 289–331, Wiley, New York.

Carver, J. P., Cumming, D. A., & Grey, A. A. (1987) in *Glycoprotein Structure and Conformation* (Ivatt, R., Ed.) Plenum, New York (in press).

Castellano, S., & Bothner-By, A. A. (1963) *J. Chem. Phys. 41*, 3863–3869.

Cooper, J. W. (1979) in *Spectroscopic Techniques for Organic Chemists*, pp 339–355, Wiley, New York.

Cumming, D. A., & Carver, J. P. (1987a) *Biochemistry* (second paper of three is this issue).

Cumming, D. A., & Carver, J. P. (1987b) *Biochemistry* (third paper of three in this issue).

Cumming, D. A., Dime, D. S., Grey, A. A., Krepinsky, J. J., & Carver, J. P. (1986) *J. Biol. Chem. 261*, 3208–3213.

De Bruyn, A., & Anteunis, M. (1976) *Carbohydr. Res. 47*, 311–314.

Fournet, B., Montreuil, J., Strecker, G., Dorland, L., Haverkamp, J., Vliegenthart, J. G. F., Binette, J. P., & Schmid, K. (1978) *Biochemistry 17*, 5206–5214.

Gagnaire, D., Horton, D., & Taravel, F. (1973) *Carbohydr. Res. 27*, 363–372.

Hassel, O., & Ottar, B. (1947) *Acta Chem. Scand. 1*, 929–942.

Hayes, M. L., Serianni, A. S., & Barker, R. (1982) *Carbohydr. Res. 100*, 87–101.

Jardetzky, O. (1980) *Biochim. Biophys. Acta 621*, 227–232.

Jardetzky, O., & Roberts, G. C. K. (1981) *NMR in Molecular Biology*, Academic, New York.

Jeffrey, G. A., McMullian, R. K., & Takagi, S. (1977) *Acta Crystallogr., Sect. B: Struct. Crystallogr. Cryst. Chem. B33*, 728–737.

Lemieux, R. U. (1978) *Chem. Soc. Rev. 7*, 423–452.

Lemieux, R. U., Bock, K., Delbaere, L. T. J., Koto, S., & Rao, V. S. (1980) *Can. J. Chem. 58*, 631–653.

Levy, G., & Peat, I. (1975) *J. Magn. Reson. 18*, 500–521.

Marchessault, R. H., & Perez, S. (1979) *Biopolymers 18*, 2369–2374.

Michalski, J.-C., Strecker, G., van Halbeek, H., Dorland, L., & Vliegenthart, J. F. G. (1982) *Carbohydr. Res. 100*, 351–363.

Mo, F. (1979) *Acta Chem. Scand., Ser. A A33*, 207–218.

Montreuil, J. (1984) *Pure Appl. Chem. 56*, 859–877.

Montreuil, J., Fournet, B., Spik, G., & Strecker, G. (1978) *C. R. Seances Acad. Sci., Ser. D 287*, 873–840.

Noggle, J. H., & Schirmer, R. E. (1971) *The Nuclear Overhauser Effect*, Academic, New York.

Ohrui, H., Nishida, Y., Watanabe, M., Hori, H., & Meguro, H. (1985) *Tetrahedron Lett. 26*, 3251–3254.

Paulsen, H., Peters, T., Sinnwell, V., Lebuhn, R., & Meyer, B. (1985) *Liebigs Ann. Chem.* 489–509.

Potenzone, R., & Hopfinger, A. J. (1975) *Carbohydr. Res. 40*, 322–336.

Rademacher, T. W., Homans, S. W., Fernandes, D. L., Dwek, R. A., Mizouchi, T., Taniguchi, T., & Kobata, A. (1983) *Biochem. Soc. Trans. 11*, 132–134.

Ramachandran, G. N., & Sasisekharen, V. (1968) *Adv. Protein Chem. 23*, 283–437.

Sanders, J. K. M., & Mersh, J. D. (1983) *Prog. Nucl. Magn. Reson. Spectrosc. 15*, 353–400.

Thorgersen, H., Lemieux, R. U., Bock, K., & Meyer, B. (1982) *Can. J. Chem. 60*, 44–57.

Tvaroska, I., Perez, S., & Marchessault, R. H. (1978) *Carbohydr. Res. 61*, 97–106.

Van Halbeek, H., Dorland, L., & Vliegenthart, J. F. G. (1981) *J. Biol. Chem. 256*, 5588–5590.

Venkatachalam, C. M., & Ramachandran, G. N. (1967) in *Conformation of Biopolymers* (Ramachandran, G. M., Ed.) Vol 1, p 83, Academic, New York.

Vliegenthart, J. F. G., Dorland, L., & van Halbeek, H. (1983) *Adv. Carbohydr. Chem. Biochem. 41*, 209–374.

Vold, R. L., Waugh, J. S., Klein, M. P., & Phelps, D. E. (1968) *J. Chem. Phys. 48*, 3831–3832.